Candidate Number: 45614

Project Number: TP09

Project Title: Nonlinear Waves in Granular Crystals

Supervisor: Mason A. Porter

Word Count: 6556

Nonlinear Waves in Granular Crystals

Abstract

The properties and stabilities of various wave types are investigated in nonlinear lattices with a 'Hertz' type potential. In particular the interaction of intrinsic localized modes with other waves is studied. Evidence is provided that Fano-like resonances, observed in other nonlinear systems, cannot occur in Hertzian lattices.

1 Introduction

The majority of real systems exhibit nonlinear dynamics to one degree or another. The analytically intractable nature of many nonlinear systems meant that it was not until the advent of modern computing that we were to begin to gain a true understanding of their behaviours [1]. Granular crystals are an example of an inherently nonlinear medium. They are of particular interest to researchers at the moment due to the tunability of the degree of their nonlinearity [2, 3]. This gives the crystals potential applications as shock absorbers [4], acoustic filters [5], and more.

A specific class of nonlinear wave, supported by granular crystals, has been shown in other systems to cause a total reflection of plane waves at certain frequencies. This effect, 'Fano resonance', has been observed in both linear and weakly nonlinear systems. Examples include light in optical waveguides [6], matter waves in Bose-Einstein condensates [7], and electrons in Josephson junctions and palladium nanoparticles [7, 8]. In this report I will consider the question of whether Fano resonances are possible for sound waves in the strongly nonlinear regime of granular crystals.

This report will proceed as follows: in section 2 I will give some background to the study of granular crystals and nonlinear systems, focusing on the types of wave solution possible (2.3, 2.4), and will outline the phenomenon of Fano resonance (2.5). In section 3, I will present new results regarding the properties of certain granular crystals (3.1) and their supported nonlinear waves (3.2, 3.3). I will outline evidence that Fano resonance cannot occur in these systems (3.4). In section 4, I summarize my results and suggest future work in this area.

2 Background

2.1 Granular Crystals

Granular crystals are closely packed collections of macroscopic particles which deform and interact elastically [3]. The dynamics of such systems are nonlinear, and prove particularly interesting owing to the possibility of tuning the degree of nonlinearity by altering system parameters. This has been shown both analytically [2] and experimentally [9, 10].

Typical granular crystals will contain tens to hundreds of beads, each a few millimetres in size. Experimentally these are often held together through a statically applied precompression, or by gravity in vertical chains. The dynamics of granular crystals can be tested by placing sensors within several beads throughout the lattice, in order to measure the force at those points as a function of time.

With a precompression applied, it is possible to develop a band structure for phonon propagation in direct analogy to that encountered in solid state physics [11] (see section 3.1). A well-defined band structure will be valid only in the linear regime of a granular crystal: that is, for small amplitude disturbances. I will refer to the allowed states of small amplitude waves as the 'linear spectrum' of a crystal lattice. A typical timescale for phonon propagation in the granular crystal will be of order milliseconds, giving some degree of controllability on the macroscopic scale.

2.2 Lattice Models

2.2.1 The Discrete Nonlinear Schrödinger System

The Discrete Nonlinear Schrödinger equation (DNLS) is a first-order wave equation. Weakly nonlinear systems governed by the DNLS have been well studied, making them a useful starting point before considering strongly nonlinear lattices [12]. The nonlinearity of the DNLS can be restricted to a subset of the lattice sites, and can be made to saturate at large amplitudes, giving the saturable DNLS (or s-DNLS) [6]. For amplitudes u_n, with a one-site saturable nonlinearity at n_i, the equations of motion are:

$$-i\frac{\partial u_n}{\partial t} = (u_{n+1} + u_{n-1}) + \left(\epsilon - \frac{\beta}{1+|u_n|^2}\right) u_n \delta_{n,n_i} \tag{1}$$

where ϵ and β give the strengths of the linear and nonlinear defects at n_i, respectively, and t is the time [6]. The DNLS has been extensively studied for its application to the propagation of light in optical waveguides [6, 13] and to the dynamics of Bose-Einstein condensates [14]. Localized to a single site as above, the s-DNLS can be used to model polarons in dielectric crystals [15].

2.2.2 Klein-Gordon Lattices

A general class of lattices is described by a discrete analogue of the Klein-Gordon equation of relativistic quantum mechanics. This class of lattices can be described by a classical Hamiltonian of the form

$$\mathcal{H}(p,q) = \sum_{i\neq j} \frac{p_i^2}{2} + V(q_i) + W(q_i - q_j) \tag{2}$$

where p and q are generalized momenta and coordinates, respectively (see, for example, [16]). The function $V(q_i)$ gives an on-site potential while the function $W(q_i - q_j)$ gives a potential between sites, usually restricted to nearest neighbours. By expanding the potentials of a system as a Taylor series it is often possible to describe it approximately by such a Hamiltonian.

2.2.3 Hertzian Lattices

In this paper I will be concerned with horizontal 1D granular crystals in which a nearest neighbour 'Hertz' potential operates. The lattice is occupied by coupled nonlinear oscillators, with nearest neighbour sites interacting via a potential of the form $W(x) \sim x^{5/2}$ where x is the displacement from equilibrium separation. The exponent is derived purely from the geometry of elastically deformable spheres in contact [17]. The equations of motion for a chain of beads, with displacements u_n from static equilibrium, take the form

$$\begin{aligned} m_n\ddot{u}_n &= A\left[\delta + (u_{n-1} - u_n)\right]_+^{3/2} \\ &\quad -A\left[\delta + (u_n - u_{n+1})\right]_+^{3/2} \end{aligned} \tag{3}$$

where the subscripted $+$ of the square brackets indicates that they return 0 if their contents are less than or equal to 0 (and hence the beads are not in contact) [3]. Here m_n is the mass of the n^{th} bead and A is a constant depending on the material and geometric properties of the beads. The value of A will differ at the end sites of the crystal depending on the boundary conditions. The static displacement of the beads, δ, due to precompression of the lattice, is given by $\delta = \left(\frac{F}{A}\right)^{2/3}$ for a precompressive force F. Experimentally, F will typically range up to around 20 N [3].

The Hertz potential differs in two important ways from general Klein-Gordon systems. First, there is no on-site potential present in the Hertz system. Second, the restriction to positive values of the brackets in equation (3) complicates the lattice's dynamics. This lack of interaction of the beads when not in contact causes an inherently asymmetric potential, which plays an important role in deciding the types of disturbance supported by the lattice. By varying the precompression applied it is possible to switch the lattice dynamics from strongly nonlinear (lower precompressions) to weakly nonlinear (higher precompressions).

An important example of Hertzian lattices is that of dimer chains. In this context, 'dimer' is used to mean that the crystal is occupied by two bead types which alternate between sites. This is shown in Figure 1. The unit cell of the lattice will contain two

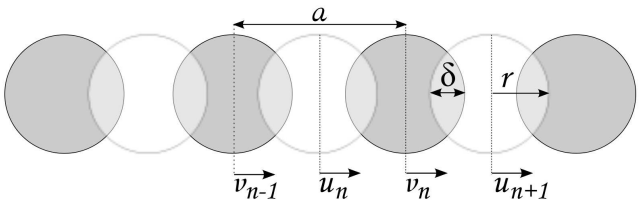

Figure 1: The displacements from static equilibrium of two bead types u and v in a dimer chain. The static overlap due to precompression is δ, and the lattice's unit cell length $a = 4r - 2\delta$.

beads; I will simplify later discussions by referring to each bead as occupying a single 'crystal site', or simply 'site'. In this report I will be focusing on a dimer chain consisting of beads with different masses but all other parameters held constant. In equation (3) this entails taking

$$m_n = \begin{cases} m_A, & n \text{ odd} \\ m_B, & n \text{ even} \end{cases}.$$

This selection fixes the value of the parameter A in the bulk crystal as:

$$A = \sqrt{\frac{8r}{9}} \left(\frac{1-\nu_A^2}{E_A} + \frac{1-\nu_B^2}{E_B} \right)^{-1} \tag{4}$$

where r is the radius of the beads, ν_A (ν_B) is the Poisson's ratio of beads A (B), and E_A (E_B) is the Young's modulus of beads A (B) [3]. The Poisson's ratio of a material is the transverse expansion caused by an axial compression of unit size; the Young's modulus is a measure of a material's stiffness [18].

The equations of motion (equation (3)) are non-dissipative. While real Hertzian lattices are found to dissipate energy over time, as would be expected, the exact mechanism of this dissipation is not yet known. Some attempts have been made to address this problem [19] but, as yet, no theory has been constructed which models correctly the observed results.

2.3 Solitary Waves

A solitary wave extends over a finite region of space and maintains its shape over a long period of time. In physics the term 'soliton' is often used interchangeably with 'solitary wave'. Mathematicians reserve the former term for a subset of solitary waves which travel and which vary by at most a change in phase upon interaction with one another [20, 21].

Solitary waves are made possible in nonlinear systems, both discrete and continuous, by the balance of nonlinearity and dispersion. A common feature of nonlinear systems is that the amplitude of a propagating disturbance is a function of its velocity. This can lead to the bunching of a wave packet as it moves. In dispersive systems the velocity of a wave is a function of its frequency, which leads to the spreading out of a wave packet of finite width (which will necessarily contain a mixture of frequencies in accordance with Fourier analysis). If a wave packet of the appropriate shape is created in a nonlinear system, the bunching effect of nonlinearity can exactly cancel the separating effect of dispersion, leading to a wave of constant shape.

The properties of solitary waves depend on the system in which they exist. In systems governed by the DNLS (section 2.2.1), solitary-wave solutions will take the form of plane waves of a single frequency attenuated inside an envelope. In a Hertzian chain, solitary waves travel as a region of compression in the crystal (see section 3.2). In this case, dimensional analysis of equation (3) gives a scaling $v_g \sim v^{1/5}$ where v_g is the group velocity of the solitary wave and v is the maximum velocity induced in a lattice bead. This result has previously been verified experimentally and numerically [9]. Solitary waves of various forms are pictured in sections 3.2 and 3.4.2.

2.4 Intrinsic Localized Modes

Intrinsic localized modes (ILMs), also called discrete breathers, are time-periodic, spatially-localized disturbances on a lattice. 'Intrinsic' in this case refers to the fact that these solutions require neither a physical inhomogeneity in the system nor an externally applied driving term; rather, their existence is made possible by the interplay between the spatial discreteness of the lattice and the nonlinearity in the lattice's governing equations. ILMs are generally localized to a few lattice sites, and are independent of the system size (provided it is larger than the ILM localization). The stability of ILMs has been proven

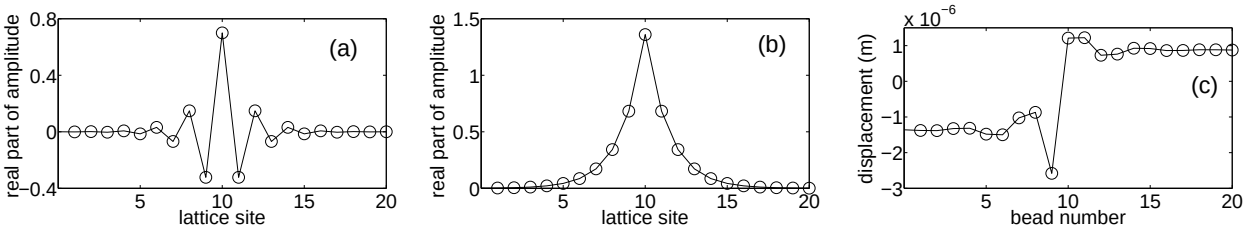

Figure 2: Some ILM types in different lattices: (a),(b) (after [6]) staggered and unstaggered modes in an s-DNLS lattice, where the complex amplitude is scaled to be dimensionless; (c) an asymmetric mode in a Hertzian lattice with 8 N precompression applied.

for a wide range of conditions [22], independent of lattice dimension and inter-site interaction.

ILM amplitudes must be relatively large in order for the nonlinearities in the equations of motion to be significant. In granular crystals, typical ILM amplitudes will be of order 10^{-6} m. In contrast, linear waves propagate in such systems at amplitudes of around 10^{-8} m. The frequency of an ILM must lie outside the linear spectrum of its lattice. If this is not the case, the ILM will radiate energy via plane waves [23].

Different systems support distinct classes of ILM. Systems governed by the s-DNLS admit both staggered and unstaggered solutions, whereas the latter are not present in lattices with Hertzian potentials. ILMs in Hertzian lattices are necessarily asymmetric [3] whereas this condition does not apply to s-DNLS lattices. Some ILM solutions are given in Figure 2.

2.5 Fano Resonances

In a general sense, for systems in which a transmission spectrum is relevant, a Fano resonance is an asymmetric transmission profile caused by the interaction of a discrete state with a continuum [24]. This phenomenon is perhaps most famously associated with atomic physics where, for example, the absorption profile of light by an atom with a single highly excited electron (a 'Rydberg atom') has a strong asymmetry [7]. In this case, the excited electron has a discrete set of states available to it, whereas the incident light can occupy a continuum of states.

The lineshape of the Fano resonance can be derived for a linear system of two coupled harmonic oscillators in which one oscillator is driven by an external sinusoidal force. The equations of motion of the oscillators are given by

$$\begin{aligned} \ddot{x}_1 + \gamma_1 \dot{x}_1 + \omega_1^2 x_1 + \nu_{12} x_2 &= a_1 \exp(i\omega t) \\ \ddot{x}_2 + \gamma_2 \dot{x}_2 + \omega_2^2 x_2 + \nu_{12} x_1 &= 0 \end{aligned} \tag{5}$$

where x_j ($j \in [1,2]$) are generalized displacements, γ_j are damping terms, and ω_j are the resonant frequencies of the uncoupled oscillators [25]. The coupling between the oscillators is ν_{12}, and a_1 is the amplitude of the sinusoidal driving term applied to oscillator 1. Substituting the ansatz

$$x_j(t) = x_j^0 \exp(i\omega t)$$

yields the solution

$$\begin{pmatrix} x_1^0 \\ x_2^0 \end{pmatrix} = \frac{1}{\Delta} \begin{pmatrix} (-\omega^2 + i\omega\gamma_2 + \omega_2^2)\, a_1 \\ -\nu_{12}\, a_1 \end{pmatrix} \tag{6}$$

where

$$\Delta = \frac{1}{(-\omega^2 + i\omega\gamma_1 + \omega_1^2)(-\omega^2 + i\omega\gamma_2 + \omega_2^2) - \nu_{12}^2}.$$

Following [25], we set $\gamma_2 = 0$ (no damping of the second oscillator), $\gamma_1 = 0.025$, and $\nu_{12} = 0.1$. The eigenfrequencies of the uncoupled system are taken to be $\omega_1 = 1$ and $\omega_2 = 1.21$. Figure 3 shows a plot of the amplitude $|x_1^0|$ as a function of the driving frequency ω (units of ω_1). The resonant frequencies are shifted slightly from the uncoupled case, and physically represent the oscillators moving either in phase or in antiphase. Around $\omega = 1.21$ the asymmetric profile of the Fano resonance can be seen, including

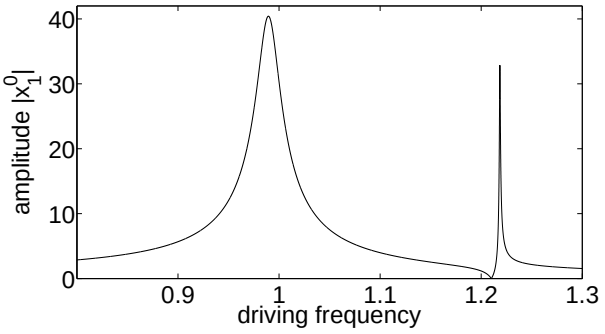

Figure 3: From equation (6), the amplitude $|x_1^0|$ (units of a/ω_1^2) of a sinusoidally driven simple harmonic oscillator when coupled to a second, undriven, oscillator as a function of driving frequency (units of ω_1). The asymmetric lineshape about frequency 1.21, including a point of zero amplitude, is characteristic of a Fano resonance.

a point of zero amplitude. In the general case this corresponds to a zero in the transmission spectrum of the system, and is the (experimentally testable) signature of a Fano resonance.

The phenomenon of Fano resonance has been observed in many weakly nonlinear systems capable of supporting ILMs, such as the s-DNLS system and Klein-Gordon lattices [6, 23, 26]. It has not so far been observed in strongly nonlinear systems.

When plane waves approach an ILM, the nonlinear interaction can generate new modes on a discrete ladder of frequencies [27]. These frequencies can lie either in the linear bands ('open channels') or in the band gaps ('closed channels'). Perhaps counterintuitively it is the *closed* channels which can lead to resonant reflection in a system. The interaction of the ILM with a closed channel generates an exponentially localized state. When the frequency of the incident wave resonates with this localized state, total reflection can occur [23, 28].

3 Results and Discussion

3.1 Dynamics of the Dimer Hertzian Lattice

In this paper, I study a Hertzian granular crystal consisting of beads with alternating masses. The equations of motion of the system, from equations (3) and (4), are given by:

$$\begin{aligned} m_u\ddot{u}_n &= A\left[\delta + v_{n-1} - u_n\right]_+^{3/2} - A\left[\delta + u_n - v_n\right]_+^{3/2} \\ m_v\ddot{v}_n &= A\left[\delta + u_n - v_n\right]_+^{3/2} - A\left[\delta + v_n - u_{n+1}\right]_+^{3/2} \end{aligned} \quad (7)$$

where the displacements are defined in Figure 1. At displacements with small amplitudes relative to those due to precompression, the contents of the brackets will not be able to become negative, so the $+$ subscript can be dropped. Factoring out δ and expanding the result to first order gives the linearized equations:

$$\begin{aligned} m_u\ddot{u}_n &\simeq \frac{3A\delta^{1/2}}{2}\left(v_n + v_{n-1} - 2u_n\right) \\ m_v\ddot{v}_n &\simeq \frac{3A\delta^{1/2}}{2}\left(u_{n+1} + u_n - 2v_n\right). \end{aligned} \quad (8)$$

Substituting the plane wave ansatz $u_n = u_0\exp\left(ikna - 2\pi ift\right)$ and $v_n = v_0\exp\left(ikna - 2\pi ift\right)$, where k is the wave number, f is the frequency, and $a = 4r - 2\delta$ is the size of one unit cell of the lattice, yields the equation

$$\begin{pmatrix} \frac{f^2}{p_u} - 2 & \exp\left(-ika\right) + 1 \\ \exp\left(ika\right) + 1 & \frac{f^2}{p_v} - 2 \end{pmatrix} \begin{pmatrix} u_0 \\ v_0 \end{pmatrix} = \vec{0} \quad (9)$$

where $p_i = 3A\delta^{1/2}/4\pi^2 m_i$ $(i = u, v)$. For nontrivial solutions, the determinant of the matrix must be zero. Applying this condition and simplifying the result gives

$$f^2 = p_u + p_v \pm \sqrt{p_u^2 + p_v^2 + 2p_u p_v\cos\left(ka\right)} \quad (10)$$

which gives the dispersion relation for the two linear phonon bands. In analogy with solid state physics the upper and lower bands are named the optic and acoustic bands, respectively. The band edges are found at $k = 0, \pm\pi/a$. Using this information, and substituting the values of p_i (with $\delta = (F/A)^{2/3}$), gives the results:

Band edge	Frequency (2 d.p.)
Lower Acoustic	$f_1 = 0.00$ kHz
Upper Acoustic	$f_2 = 4.71$ kHz
Lower Optic	$f_3 = 8.10$ kHz
Upper Optic	$f_4 = 9.37$ kHz

Table 1: The theoretical frequencies of the linear band edges at 20 N precompression.

$$
\begin{aligned}
f_1 &= 0 \quad \text{(lower acoustic)} \\
f_2 &= \sqrt{\frac{3A^{2/3}F^{1/3}}{4\pi^2 m_u}} \quad \text{(upper acoustic)} \\
f_3 &= \sqrt{\frac{3A^{2/3}F^{1/3}}{4\pi^2 m_v}} \quad \text{(lower optic)} \\
f_4 &= \sqrt{\frac{3A^{2/3}F^{1/3}}{4\pi^2}\left(\frac{1}{m_u}+\frac{1}{m_v}\right)} \quad \text{(upper optic)}
\end{aligned}
$$

where $m_v < m_u$ (without loss of generality). Physically these band edges correspond to the following situations: f_1 has all the beads moving together with zero velocity; f_2 has the light beads stationary and the heavy beads oscillating, with heavy beads in adjacent unit cells in antiphase; f_3 has the situation reversed with heavy beads stationary and light beads oscillating; f_4 has all the heavy beads moving together in phase, and all the light beads moving together in antiphase with them. The relative amplitudes of oscillation are such that the crystal's centre of mass is stationary in each case.

I follow [3] by choosing beads A to be made of aluminium and beads B to be made of stainless steel. From [3] and references therein this gives parameter values $v_A = 0.33$, $v_B = 0.30$, $E_A = 73.5$ GPa, and $E_B = 193$ GPa. The bead radii are taken to be $r = 9.525$ mm, giving $m_u = 28.84$ g, $m_v = 9.75$ g. Using these values in a lattice with 20 N precompressive force F gives the band edge frequencies of Table 1. The dispersion relation of equation (10) is plotted in Figure 4 (a).

I then checked these analytic results numerically by testing the properties of a simulated 299 bead crystal of the above specifications. Both ends of the crystal were beads of type A (aluminium). Site 1 of the crystal was held stationary, simulating an immovable aluminium wall. The displacement of site 299 was allowed to be varied externally, representing an actuator driving the system. The precompression was held at 20 N.

I first checked the response of the crystal to small amplitude (10^{-8} m) plane waves, by sinusoidally varying the displacement of bead 299 with frequencies in the range of 0-12 kHz at intervals of 100 Hz. The driving force was applied for 11 ms in each case. Within the acoustic band this was sufficient time for the waves to reach site 70. At other frequencies the situation was not so clear cut. At band edges other than f_1 the group velocity $\frac{\partial\omega}{\partial k}$ of plane waves tends to zero, but the phase velocity $\frac{\omega}{k}$ does not (here $\omega = 2\pi f$). This causes a distortion of the waves' shapes, and time dependent amplitudes, along the lattice.

I chose to take the amplitude to be the average between sites 1 and 297, as measured at 11 ms. The amplitudes of the two end beads were representative of the driving force rather than of the crystal itself. The result is shown, after dividing by the driving amplitude, in Figure 4 (b). No waves could traverse the lattice completely in this time, so the values found are necessarily an underestimate. Furthermore, with waves of different frequency travelling different distances in 11 ms, a systematic error will have been introduced. On the other hand, the result gives a good qualitative description of the crystal's response at each frequency. An attempt to average the amplitudes only over the distance traversed by each wave would give a significant overestimate around band edges, leading to an unrepresentative shape of the transmission spectrum.

As a second test on the analytic results, I calculated the temporal Fourier transform of the amplitude at sites 150 and 151, after applying uniformly-distributed random displacements in the range $\left[-10^{-8}\text{ m},\ 10^{-8}\text{ m}\right]$ to all beads in the bulk crystal. The end beads were held stationary. In order to find a representative response of a crystal unit cell it was necessary to sample neighbouring odd and even sites. The resulting spectrum, Figure 4 (c), shows the relative contributions of plane waves at each frequency to the motion of the crystal during the 242 ms sample time. The validity of the Fourier transform is discussed in section 3.4.2.

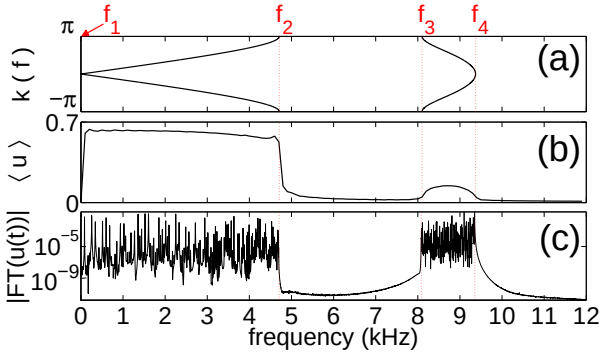

Figure 4: Analytic and numerical results for the small amplitude (10^{-8} m) response of the crystal of section 3.1 at 20 N precompression. (a) The analytically calculated (inverse) dispersion relation $k(f)$. (b) The average amplitude $\langle u \rangle$ of plane waves in the bulk crystal upon sinusoidally driving the end bead for 11 ms, normalized to the driving amplitude. (c) The absolute value of the Fourier transform of the amplitudes of one unit cell, $u(t)$, after initially randomly displacing the crystal's beads (plotted on a logarithmic scale). This test was run for 242 ms. All figures share a common x axis, and the calculated band edges of Table 1 have been indicated.

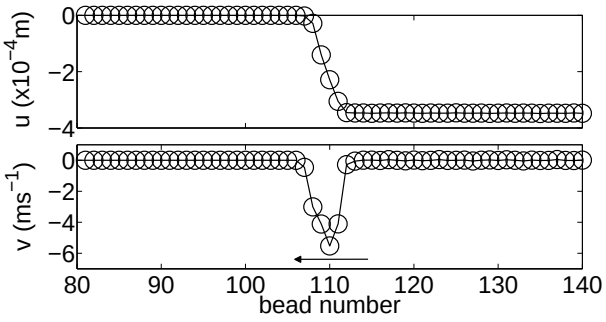

Figure 5: The displacements u and velocities v of the beads in a crystal struck at site 298 by an aluminium bead travelling at -20 ms^{-1}. The resulting solitary wave induces a kink into the crystal as it propagates. The lattice had 8 N precompression applied, and the test had run for 3.8 ms at this point. The graphs share a common x axis. The circles mark bead locations but do not represent bead sizes.

3.2 Solitary Wave Solutions

Solitary waves arise from a balance between nonlinearity and dispersion (section 2.3). This fact suggests that in order for a solitary wave to be stable its amplitude must be large enough to be significantly affected by the nonlinear terms in the equations of motion. In comparison, plane waves are only stable in the small amplitude limit.

The dimer Hertzian lattice provides a useful setting for testing the stability of different solutions, as the degree of nonlinearity can be varied by altering the lattice's precompression. For a given amplitude, plane waves become more stable at higher precompressions and solitary waves become more stable at lower precompressions. I was able to verify this statement numerically by applying an impulse to the end bead of the simulated 299 bead crystal of section 3.1. This was implemented by starting the end bead with a nonzero velocity but zero displacement. Physically this situation represents an aluminium bead (site 299) being rolled into the end (stainless steel) bead, now site 298, of the crystal and contacting at time $t = 0$.

At zero lattice precompression, solitary waves are stable at all amplitudes and plane waves cannot propagate. This is a consequence of the asymmetric inter-site potential. At a given striker bead velocity, as the precompression in the lattice is turned up, a solitary wave will gradually gain a 'tail' of further solitary waves. These separate solitary waves eventually coalesce into a plane wave as the precompression increases and causes the lattice to become linear at the amplitude of the disturbance.

Viewed from the opposite perspective, if the system parameters are chosen such that the striker bead sets up a good approximation to a plane wave, this wave will separate into individual solitary waves as the precompression is decreased. As a guide to some typical parameter values, in a lattice with 20 N precompression the striking bead must hit at around 0.4 ms^{-1} or higher to create a stable solitary wave. This value drops to around 0.1 ms^{-1} for 5 N precompression, and 0.03 ms^{-1} for 1 N precompression. Solitary waves induced by this method are known as 'kinks', on account of the fact that they cause a net displacement of the beads they have travelled through. An example of a stable kink is given in Figure 5.

Given a sufficiently long time in a large lattice, any short impulse of the form just described will eventually lead to a sequence of approximately isolated solitary waves. This is due to the dependence of the waves' group velocity on the velocity of the individual beads described in section 2.3. This can provide a method of creating small amplitude solitary waves, by allowing small amplitude (approximate) plane waves to separate out over a large lattice length.

In numerical simulations, it is possible to create solitary waves by a different method. This is to set up a crystal with a Gaussian distribution of starting displacements, and all initial velocities zero. Provided the Gaussian is wide enough (around 10 sites full width at half maximum) it will decay into two oppositely directed solitary waves. The waves take the shape of the original envelope, but scaled down to conserve energy. This method is very versatile and can be used to create arbitrarily small solitary waves, in lattices of arbitrarily high precompression. This provides an extremely useful tool in the search for Fano resonances (section 3.4).

Non-Gaussian starting configurations can also work to create solitary waves, but with varying degrees of success. Lorentzian envelopes, defined by

$$u_n = a\frac{\gamma^2}{(n-n_0)^2+\gamma^2}$$

with a the packet's amplitude, γ the full width at half maximum (FWHM), and n_0 the centre of the distribution, must have a FWHM greater than around 20 sites to give stable solitary waves. If this condition is fulfilled, the resulting waves will have a Lorentzian shape. A 'Top Hat' function of the form

$$u_n = \begin{cases} a, & n_1 < n < n_2 \\ 0, & \text{otherwise} \end{cases}$$

will give solitary waves with long tails approaching plane waves.

From observation of many starting configurations I have inferred that if the initial envelope or its first derivative are discontinuous at any point this will result in solitary waves tailed by plane waves. If the distribution and its first derivative are approximately continuous throughout the lattice, this will result in solitary waves with little or no noise, and no plane wave tail. Both the numerical model and the real lattice being described are discrete systems, so this stability condition is more accurately described by how sharply the functions or their first derivatives vary. This gives the minimum widths of the Gaussian and Lorentzian envelopes. The starting configuration need not be symmetric: whatever distribution is chosen, two smaller amplitude replicas will form and counter-propagate. An example is given in Figure 6.

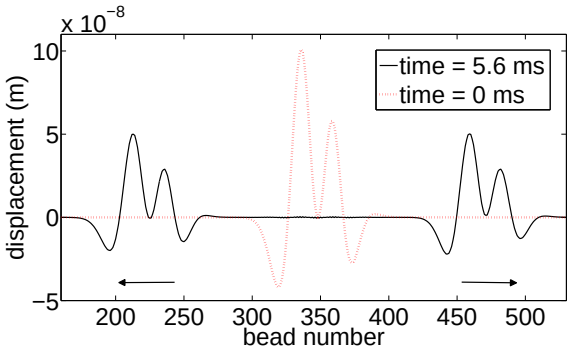

Figure 6: A spatially continuous starting configuration (red, dashed), with continuous first derivative, leads to two counter-propagating solitary waves (black, solid). The directions of propagation of the waves are indicated. This 699 bead dimer Hertzian lattice had 8 N precompression applied.

3.3 ILMs in the Dimer Hertzian Lattice

Stable intrinsic localized modes exist in Hertzian lattices for a range of conditions. The frequencies of oscillation of all ILMs found so far have been outside the linear spectrum of their lattice. In this report I have worked with ILMs whose frequencies are located between the acoustic and optic bands.

Experimentally, ILMs can be induced by applying a small amplitude sinusoidal driving force to the end bead of a precompressed crystal. Driving the crystal at the frequency of a band edge can lead to ILM formation in the neighbouring band gap by a phenomenon known as Modulational Instability [29]. The experimental signature of these ILMs is a peak in the Fourier spectrum of the ILM sites at a frequency within the band gap, found by placing a force sensor within the appropriate bead [3].

In numerical simulations it is possible to set up a crystal with the correct displacements and velocities at each site so as to cause a stable ILM. I developed an effective method of finding these starting conditions: I enclosed uniformly-distributed random displacements, in the range $\left[-5 \times 10^{-6} \text{ m}, 5 \times 10^{-6} \text{ m}\right]$, in an envelope of width around 10 crystal sites in the centre of a large lattice (different envelopes vary slightly in success rate, and I found Gaussians to work most effectively). I set all velocities to zero. I allowed this initial configuration to evolve until the resulting noise had spread out to the ends of the crystal. By conservation of energy the noise around the centre of the crystal decreased in amplitude.

An ILM will result from this method in the majority of cases. In those cases where an ILM is not created it is generally due to the fact that a band edge mode (section 3.1) has been activated instead. In this case the mode will eventually spread throughout the crystal. Looking at the form of ILM solutions as a function of their frequency reveals that, as the frequency approaches a band edge, the number of sites occupied by the ILM increases, tending to the system size as $f \to f_{\text{band edge}}$ [3]. To this extent band edge modes can be thought of as the large width limit of stable ILM solutions.

Once an ILM is generated, the displacements of the beads not contributing to the oscillation can be set to zero and the simulation run again. Each time this process is repeated, the noise present in the surrounding crystal will be diminished. Iterating until the noise is smaller than any signals of interest results in a stable ILM which can be used in further tests. An example of such a stable ILM is shown in Figure 2 (c).

The frequencies of oscillation of the ILMs generated by this method are shown in Figure 7. To date, only ILMs whose frequencies lie in the lower band gap have been found in Hertzian lattices. If ILMs can exist in the upper band gap it would seem probable that their form will be different from that of the lower band gap solutions. If not, the method outlined above would be expected occasionally to generate ILMs of upper band gap frequencies, which I have not found to be the case. Alternatives to the types of ILM solution found so far could include so-called 'dark breathers', in which the displacements

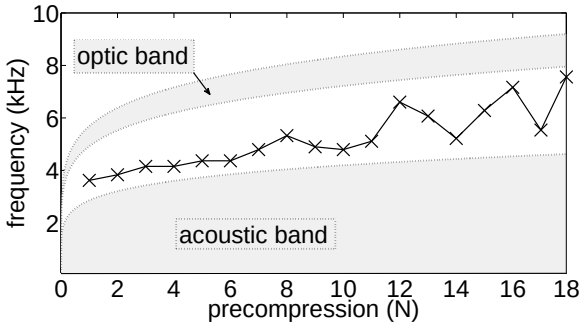

Figure 7: The oscillation frequencies of ILMs generated by the method of section 3.3 (crosses). The analytically calculated linear bands are shown for reference.

of the ILM sites are smaller than in the surrounding crystal. This is in analogy to the 'dark solitons' observed in many systems. The existence of dark breathers has been demonstrated in Klein-Gordon lattices (section 2.2.2) for a range of conditions [30].

3.4 Fano Resonance Results

In their extensive review of ILMs [23], Flach and Gorbach study the conditions necessary for Fano resonance in systems with potentials of the form

$$V(x) = 0;\ W(x) = \phi_2 \frac{x^2}{2} + \phi_3 \frac{x^3}{3} + \phi_4 \frac{x^4}{4} \qquad (11)$$

where $V(x)$ is an on-site potential and $W(x)$ is between nearest neighbours. They deduce that bond-centred, as opposed to bead-centred, ILMs are required for such a resonance. The Hertz potential can be approximated to the above form by a truncated Taylor series, although this approximation neglects the inbuilt zero tensile response of equation (3). None of the ILMs I have encountered in this study have been bond-centred.

I employed two methods in a numerical search for Fano resonances in a simulated dimer Hertzian lattice. The first was to test the transmission properties of ILMs to plane waves of individual frequencies. The second was to test the transmission spectra of ILMs to broadband wave packets in the form of solitary waves.

In both tests the crystal was of the prescription given in section 3.1. By the method of section 3.3, I was able to stabilize ILMs in the crystal at various precompressions. All ILMs were localized to fewer than 10 sites, and the noise in the surrounding crystal was of amplitude less than 5×10^{-9} m in all cases.

3.4.1 Plane Wave Transmission

This test consisted of applying a small amplitude (10^{-8} m) sinusoidal driving force to the end bead of a 299 bead crystal containing an ILM around site 150. An advantage of this method is that individual frequencies can be tested to arbitrary resolution by varying the step in incident frequency between runs. Furthermore, the displacements and velocities of individual beads can be found, giving a good physical picture of what is happening in the wave-ILM interaction.

The transmission spectrum for plane waves in the absence of ILMs for 20 N precompression is given in Figure 4 (b). The occurrence of a Fano resonance in the presence of ILMs would be signalled by a drop to zero of the transmitted wave amplitude within a linear band. I conducted tests in lattices with precompressions from 1 N to 20 N, in steps of 1 N, and at some higher (experimentally unattainable) forces.

A representative example of the results obtained is given in Figure 8, which shows the transmission properties of a crystal with 8 N precompression. The graph was obtained as follows: within the acoustic band and band gaps, the crystal was driven for 12.7 ms at site 299. At these frequencies this was long enough for the waves comfortably to reach site 50, where the ILM (when present) was located at site 150. The amplitude was averaged between sites 50 and 140. Within the optic band it was necessary to drive the crystal for a longer time to get a representative transmitted wave. This was because the optic band is rather narrow, so the states within it are always close to a band edge. The group velocities are therefore quite small. In the range 6900 Hz - 8100 Hz the crystal was driven for 37.6 ms, which was long enough for the waves to reach site 100. The average amplitude in this case was taken between sites 100 and 140. The peaks in both spectra at the upper acoustic band edge are a relic of averaging only over a region of the crystal containing the waves (*cf.* section 3.1).

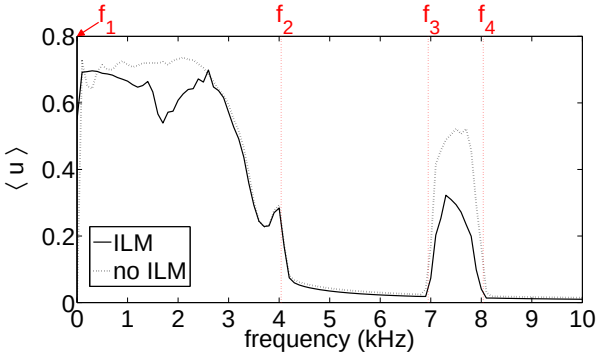

Figure 8: The amplitude of transmitted waves divided by the driving amplitude (10^{-8} m) in a crystal with 8 N precompression. The dashed line shows the crystal's response in the absence of an ILM. The solid line shows the response in the presence of an ILM, after subtracting the disturbance due to the ILM itself. The analytically calculated band edges are indicated.

While Figure 8 shows a reduced transmission in the presence of an ILM, at no point does this transmission drop to zero. For this reason, it would seem a Fano resonance is not occurring in this system. Applying the same test over the aforementioned range of precompressions yields the same result in each case. Inductively this supports the conclusion that ILMs in Hertzian lattices are unable to demonstrate Fano resonance.

3.4.2 Solitary Wave Transmission

The basic principle of Fourier analysis is that any function with at most a finite number of discontinuities can be decomposed into harmonics (which will take the form of sinusoidal waves in systems of interest to this study). This is true in systems where linear superposition applies[1]. In nonlinear granular crystals this is not strictly the case, but for small amplitude waves linear superposition holds approximately. For this reason, solitary waves can

[1]Strictly speaking the Fourier transform applies to continuous systems of infinite size. The approximate method of Discrete (or Finite) Fourier Transforms is relevant to the systems of interest here. See, for example, [31].

be thought of as a collection of plane waves linearly superposed. The spatial Fourier transform (FT) of a solitary wave will give the contribution of each different wave number of plane wave to the packet. Wave number and frequency can be related in this system by the dispersion relation of equation (10). If a Fano resonance were to occur at some frequency when passing a solitary wave through an ILM, the corresponding wave number would be absent from the FT of the transmitted wave packet. This would change the shape of the solitary wave, and could destabilize it.

A Gaussian solitary wave will contain a Gaussian distribution of wave numbers, with thin distributions in real space giving wide distributions in k space. A delta function in real space, which can be thought of as the limit of an infinitely thin distribution, would contain equal amounts of all wave numbers, but this configuration is not a stable solitary wave. As a compromise, I chose to employ the thinnest real space Gaussian distribution attainable, with a width of 10 sites FWHM.

By Fourier transforming the shape of this solitary wave, I found the distribution in k space to cover the approximate range $k \in [-0.13\pi,\ 0.13\pi]$, *i.e.* the wave was composed of wave numbers from the lowest 13% of the possible domain. By comparing with the dispersion graph 4 (a) it can be seen that this range covers the lower part of the acoustic band and the upper part of the optic band. The lack of total coverage is a clear disadvantage to this method, but the domain which *is* covered is sampled with the greatest possible resolution.

I carried out the test numerically by modelling a 299 bead crystal with 8 N precompression and an ILM (amplitude 2×10^{-6} m) around site 150. I centred a solitary wave (amplitude 5×10^{-9} m) at site 250, and allowed it to propagate through the ILM. For clarity, I then subtracted the disturbance due to the ILM itself. The result is shown in Figure 9. Some of the solitary wave reflects in the form of a solitary wave of a different shape. It should be noted that after repeated tests of the reflected wave, using incident Gaussian solitary waves of different widths, I found that it is not an attenuated plane wave (despite the similarity in appearance).

The transmitted wave loses some height by conservation of energy, and consequently has a reduced

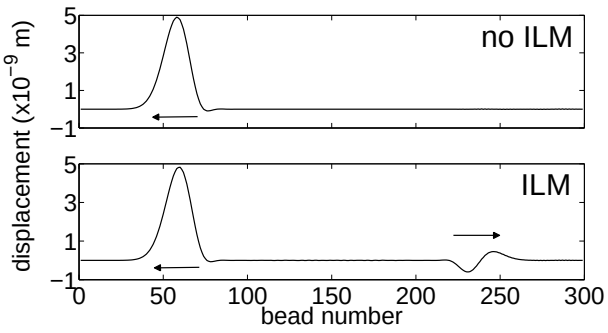

Figure 9: The displacements of the beads after starting a left travelling solitary wave around bead 250 and running for 9.4 ms. Part of the solitary wave reflects in the presence of an ILM (lower figure; ILM disturbance subtracted). The amplitude of the transmitted wave is reduced to conserve energy, but the shape is unchanged relative to the non-interacting case (upper figure). The graphs share common axes.

velocity relative to the non-interacting case. By Fourier transforming the transmitted waves I was able to confirm that the distributions of wave numbers are identical in each case. This demonstrates the absence of a Fano resonance in the range of wave numbers sampled by the solitary wave for 8 N precompression. The same test was applied for various precompressions with the same result in each case.

4 Conclusions

In this report I have developed new methods for creating and stabilizing solitary waves and intrinsic localized modes in numerical models of granular crystals. I have applied these methods to the study of Fano resonance in lattices with a Hertzian potential and have found no evidence that such resonances can be supported.

I believe future work in the study of Fano resonances in Hertzian lattices should be directed towards finding new forms of ILM, such as 'bond-centred' forms (section 3.4) or 'dark' forms (section 3.3). A good starting point may be to search for such solutions in the upper band gap.

Acknowledgments

I thank my supervisor Mason Porter for many useful discussions and for providing a template MATLAB code for the lattice simulations.

References

[1] M. A. Porter *et al.*, American Scientist 97, 214–221 (2009)

[2] V. F. Nesterenko, Dynamics of Heterogeneous Materials, Springer-Verlag New York (2001)

[3] N. Boechler *et al.*, arXiv 0911.2817 v1 (2009)

[4] F. Fraternali, M. A. Porter, and C. Daraio, Mech. Adv. Mat. Struct. 17, 1–19 (2010)

[5] V. F. Nesterenko *et al.*, Phys. Rev. Lett. 95, 158702 (2005)

[6] U. Naether *et al.*, Opt. Lett. 34, 2721–2723 (2009)

[7] A. E. Miroshnichenko, S. Flach, and Y. S. Kivshar, Rev. Mod. Phys. (in print), arXiv 0902.3014 v4 (2009)

[8] T. Pakizeh *et al.*, Nano Lett. 9, 882–886 (2009)

[9] M. A. Porter *et al.*, Physica D 238, 666–676 (2009)

[10] G. Theocharis *et al.*, Phys. Rev. E 80, 066601 (2009)

[11] C. Kittel, Introduction to Solid State Physics, 8^{th} ed., Wiley (2005)

[12] J. C. Eilbeck and M. Johansson in: L. Vázquez *et al.* (Ed.), Proc. of the 3rd Conf. Localization & Energy Transfer in Nonlinear Systems, World Scientific, New Jersey, 44–67 (2003) (arXiv:nlin/0211049v1)

[13] H. S. Eisenberg and Y. Silberberg, Phys. Rev. Lett. 81, 3383–3386 (1998)

[14] A. Trombettoni and A. Smerzi, Phys. Rev. Lett. 86, 2353–2356 (2001)

[15] T. Holstein, Ann. Phys. NY 8, 325–342 (1959)

[16] L. D. Landau and E. M. Lifshitz, Mechanics, 3^{rd} ed., Pergamon Press, Oxford (1960)

[17] K. L. Johnson, Contact Mechanics, Cambridge University Press (1985)

[18] M. F. Ashby and D. R. H. Jones, Engineering Materials 1, 3^{rd} ed., Butterworth-Heinemann (2005)

[19] R. Carretero-González *et al.*, Phys. Rev. Lett. 102, 024102 (2009)

[20] P. G. Drazin and R. S. Johnson, Solitons: An introduction, Cambridge University Press (1989)

[21] A. C. Scott (Ed.), Encyclopedia of Nonlinear Science, Routledge, Taylor & Francis Group, New York (2005)

[22] R. S. MacKay and S. Aubry, Nonlinearity 7, 1623–1643 (1994)

[23] S. Flach and A. V. Gorbach, Phys. Rep. 467, 1–116 (2008)

[24] U. Fano, Phys. Rev. 124, 1866-1878 (1961)

[25] Y. S. Joe, A. M. Satanin, and C. S. Kim, Phys. Scr. 74, 259–266 (2006)

[26] S. Flach, A. E. Miroshnichenko, and M. V. Fistul, Chaos 13, 596–612 (2003)

[27] T. Cretegny, S. Aubry, and S. Flach, Physica D 119, 73–87 (1998)

[28] A. V. Gorbach *et al.*, Proc. SPIE, 5975, 59750V (2006)

[29] G. Huang and B. Hu, Phys. Rev. B 57, 5746–5757 (1998)

[30] A. Alvarez *et al.,* New J. Phys. 4, 72.1–72.19 (2002)

[31] W. H. Press *et al.*, Numerical Recipes: The Art of Scientific Computing, 3^{rd} ed., Cambridge University Press (2007)